Nano Research

ISSN 1998-0124 CN 11-5974/O4
https://doi.org/10.1007/s12274-023-5408-5

Research Article

Construction of twisted graphene–silicene heterostructures

Guangyuan Han[1,2], Huan Shan[1,2], Lizhi Zhang[2,3], Wenpeng Xu[1,2], Zhao-Yan Gao[1,2], Hui Guo[1,2], Geng Li[1,2,4] (✉), and Hong-Jun Gao[1,2,4]

[1] *Beijing National Center for Condensed Matter Physics and Institute of Physics, Chinese Academy of Sciences, Beijing 100190, China*
[2] *School of Physical Sciences, University of Chinese Academy of Sciences, Beijing 100190, China*
[3] *National Center for Nanoscience and Technology, Chinese Academy of Sciences, Beijing 100190, China*
[4] *Songshan Lake Materials Laboratory, Dongguan 523808, China*

Received: 12 October 2022 / **Revised:** 30 November 2022 / **Accepted:** 15 December 2022

ABSTRACT

Van der Waals stacking of two-dimensional crystals with rotation or mismatch in lattice constants gives rise to rich physical phenomena that are closely related to the strong correlations and band topology. Twisted graphene and silicene heterobilayers have been theoretically predicted to host a tunable transport gap due to the mismatch of Dirac cones in the graphene and silicene layers. However, experimental realization of such twisted structure is challenging. Here, we report the formation of twisted graphene/silicene bilayers on Ru (0001) crystal via intercalation. Different moiré patterns form as single-crystalline graphene grows over different grains of the Ru surface. After silicon intercalation, graphene/silicene bilayers are observed with different twisting angles on top of different grains of the Ru substrate. Our work provides a new pathway towards construction of graphene based twisted heterobilayers.

KEYWORDS

twisted heterobilayers, graphene, silicene, scanning tunneling microscopy, first-principles calculations

1 Introduction

The moiré materials, composed by two dimensional (2D) crystals with mismatch in lattice orientations and/or constants, act as versatile and tunable platforms for investigating exotic phenomena in condensed matter physics [1, 2]. The moiré superstructure imposes additional periodic potential to the stacked 2D systems, reshaping their band structures. Starting from the discovery of correlated insulator and superconductivity in magic-angle twisted bilayer graphene [3, 4], orbital magnetism [5], Chern insulators [6], and Wigner crystals [7], and other intriguing phenomena [8–10] have been identified in different moiré materials. So far, graphene [3–5, 11–13], hexagonal boron nitride [14], transition metal dichalcogenides [15–20], and other 2D crystals [8, 10, 21] have been employed as building blocks to construct the moiré materials.

Among the various moiré materials, the twisted graphene/silicene (TGS) heterobilayers have received lots of interest due to its fascinating physical properties. It has been predicted that the stacking of these two pieces of semi-metallic layers surprisingly leads to the formation of a semiconductor with pronounced transport gap, regardless of their relative orientation [22]. The reason is that the different lattice constants in graphene and silicene guarantee that the electron tunneling cannot happen without compensating the momentum difference at the two Dirac cones. It has also been proposed that the graphene/silicene bilayer is potentially applicable for a nanocapacitor with piezoelectric capabilities [23].

However, experimental fabrication of the TGS is challenging. On the one hand, silicon does not have a layered bulk allotrope [24] and 2D silicene cannot be fabricated using mechanical exfoliation technique [25]. On the other hand, the epitaxially-grown silicene atomic layer requires the supporting from the epitaxial substrate and cannot be transferred to other substrates. As a result, the traditional manual stacking method cannot be implemented to fabricate the graphene/silicene bilayers. It has been previously reported that graphene and silicene heterostructures can be fabricated on solid surfaces through graphene intercalation [26–28] or molecular beam epitaxy [29]. However, to the best of our knowledge, the TGS heterobilayers with controllable twisting angles have not been realized.

Here we present the construction of TGS heterobilayers with different twisting angles on Ru (0001) substrate. The Ru crystal is first treated by multiple times of high temperature (~ 1200 K) annealing and fast cooling process to create grains with different orientations on the surface (Fig. 1(a)). Monolayer graphene is then grown on the treated Ru surface through a standard epitaxial technique [30, 31]. The single-crystalline graphene stretches over different grains, giving rise to different moiré patterns (Fig. 1(b)). According to a previous density functional theory (DFT) prediction, even more orientations could exist under certain conditions [32, 33]. The silicon is then deposited and intercalated between graphene and the Ru substrate where silicene grows. The lattice orientation of silicene is determined by the Ru grains, and as a result TGS with different twisting angles forms on top of the polycrystalline Ru surface (Figs. 1(c) and 1(d)). Moreover, DFT calculations demonstrate the Si intercalation and silicene formation behaviors on the twisted region under graphene moiré

Address correspondence to gengli.iop@iphy.ac.cn

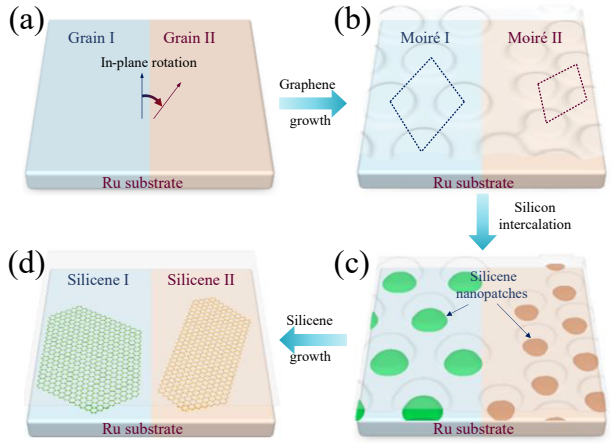

Figure 1 Schematic of the formation of the TGS heterobilayer. (a) Grains with in-plane rotations in Ru substrate form during annealing and fast cooling treatment. (b) Single crystalline graphene layer grows across the Ru grains, forming different types of moiré patterns. (c) Intercalated Si atoms form silicene nano flakes below the domes of the moiré pattern. (d) The lattice orientation of the silicene layer is locked with the underlying Ru grain, leading to TGS heterobilayers.

patterns, and provide theoretical evidence of the ordered growth of TGS.

2 Results and discussion

All the experiments were performed in an home-built low-temperature scanning probe microscopy system [34] with a base pressure below 2×10^{-10} mbar . The Ru (0001) crystal purchased from MaTeck Material Technologie & Kristalle GmbH with a diameter of 10 mm and a thickness of 0.8 mm is repeatedly sputtered with argon ion source, annealed from 300 to 1200 K in 7 min using an ultra-high vacuum electron beam heater, and fast-cooled to 300 K in 20 min to yield the polycrystalline surface. Single layer graphene is fabricated by exposing the Ru surface to ethylene with a pressure of 2×10^{-6} mbar at 1300 K [30, 31]. Si atoms were evaporated from a home-built E-beam evaporator with the calibrated evaporation rate of 0.33 monolayer/min (calibrated by a low energy electron diffraction system in the deposition tests). Intercalated silicene is realized by annealing the sample under 800 K for 30 min. The scanning tunneling microscopy (STM) images are taken under 4.2 K with chemically etched tungsten tips. Scanning tunneling spectra are acquired by keeping the feedback of Z-controller on and the sample bias being ramped from 2 to 10 V. The dI/dV signals are recorded by a lock-in amplifier with a bias modulation of 15 mV at 723 Hz [35]. The calculations were carried out using Vienna *ab initio* simulation package (VASP) [36, 37]. The projected augmented wave (PAW) method [38] was used to describe the core–valence interactions. The generalized gradient approximation (GGA) in the form of Perdew–Burke–Ernzerhof (PBE) is adopted for the exchange-correlation functional [39]. All the periodic slab models include four layers of Ru, one layer of graphene, and a vacuum layer of more than 15 Å. During the calculations, all the atoms except the bottom two layers of Ru (0001) were fully relaxed until the net force on each relaxed atom was less than 0.01 eV/Å, and a Γ point k-sampling was employed for Brillouin zone matrix integrations due to the numerical limitations.

The repeated annealing and fast cooling of the Ru crystal create randomly aligned grains. It has been shown that polycrystalline Ru film possesses multiple grains with in-plane rotations, and the epitaxial graphene grown on top of the polycrystalline film is single-crystalline [32]. Figure 2(a) shows a typical STM topography of single layer graphene stretching across three different grains of the Ru surface. Based on the current experimental technique, we normally observe grain size of ~ 100 nm (Fig. S1 in the Electronic Supplementary Material (ESM)). Occasionally, we can find regions of several hundreds of nanometers or even in micron scale. The grain boundaries can be easily differentiated given the different moiré patterns between graphene and the Ru substrate. It has been shown that graphene forms regular moiré structure on the single-crystalline Ru (0001) substrate without any rotations between the graphene and the Ru lattice (moiré pattern R0, with 11 × 11 graphene on 12 × 12 Ru in

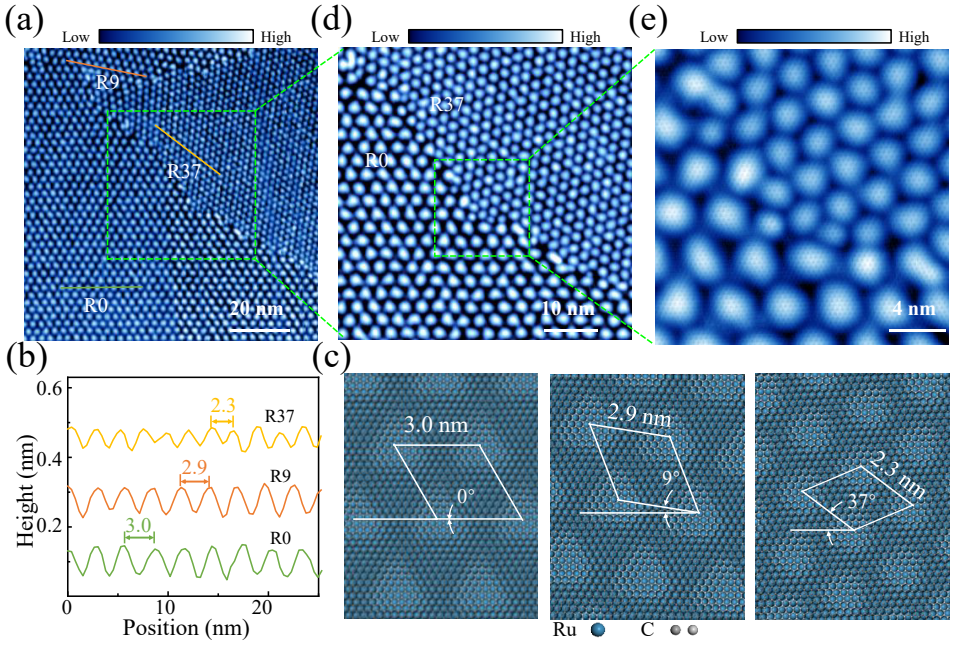

Figure 2 STM topography of graphene moiré patterns on Ru grains. (a) Large scale STM image of the R0, R9, and R37 moiré patterns of single crystalline graphene on Ru grains (scanning settings: bias $V_s = -3$ V, $I_t = 50$ pA). (b) Line profiles along the moiré patterns in the R0, R9, and R37 regions, showing different periodicity. (c) DFT simulations of moiré patterns of R0, R9, and R37 formed by different orientations between graphene and Ru lattices. (d) Zoom-in STM image of the green dashed square in (a) ($V_s = -3$ V, $I_t = 50$ pA). (e) Zoom-in STM image of the green dashed square in (d), showing single crystalline graphene across the grain boundary between the R0 and R37 regions ($V_s = -0.3$ V, $I_t = 400$ pA).

a unit cell). Due to the strong interaction between graphene and the Ru substrate, the as-grown graphene layer is single-crystalline [30, 31, 40]. However, in the presence of nano scale Ru grains, the graphene layer could either be single crystalline across Ru grains and form different moiré pattern, or rotate with the underlying Ru grains by forming one dimensional (1D) atomic defects at the grain boundaries. The structure of the graphene layer depends on the competition between the formation energy of a new moiré pattern and that of 1D atomic defect. Our calculation (Table S1 in the ESM) shows that the total energy in R37 increases ~ 1.7 meV per carbon atom as compared with that in R0, which is much smaller than the energy needed to form a 4° graphene grain boundary [41]. As a result, the graphene keeps single crystalline across the Ru grain boundary, leading to other types of moiré patterns [32, 33], e.g., moiré pattern R9 ($2\sqrt{31}\times 2\sqrt{31}$ graphene/$\sqrt{103}\times\sqrt{103}$ Ru), R19 ($\sqrt{133}\times\sqrt{133}$ graphene/$4\sqrt{7}\times 4\sqrt{7}$ Ru), R37 ($2\sqrt{19}\times 2\sqrt{19}$ graphene on $3\sqrt{7}\times 3\sqrt{7}$ Ru), and R55 (11 × 11 graphene/$7\sqrt{3}\times 7\sqrt{3}$ Ru) (Fig. 2(a) and Table S1 and Fig. S2 in the ESM). According to a previous DFT prediction [33], even more orientations could exist under certain conditions.

Notably, the moiré patterns in different grains differ not only in orientations, but also in periodicity (Figs. 2(b) and 2(c)) and corrugation. For example, the graphene ripples stronger in R0 moiré pattern region than that in R37 moiré pattern region (green and yellow curves in Fig. 2(b)). The space between the graphene domes of the moiré pattern and the Ru substrate confines electrons, leading to existence of quantum well states revealed by scanning tunneling spectroscopy (STS) [42]. The scanning tunneling spectra show a lower quantum well state on the dome of the R0 region than that on the dome of R37 region, further confirming that the spacing between the graphene dome and the substrate in the R0 structure is larger (Fig. S3 in the ESM). The formation of different moiré patterns is different from that in the epitaxial systems where the interaction between graphene and the substrate is weak [43] and polycrystalline graphene grows. In the current case, the graphene layer remains single-crystalline across grain boundaries (Figs. 2(d) and 2(e) and Fig. S4 in the ESM). Silicon intercalation happens upon annealing the silicon clusters deposited on the graphene/Ru surface [44, 45]. Due to a strong interaction between the interfacial silicon atoms and the Ru substrate, the lattice orientation of the as-grown silicene is locked with the Ru grain. As a result, rotation angles are expected between graphene and silicene at the different moiré regions. Figure 3(a) displays the STM topography of adjacent R0 and R37 regions after small amount of Si intercalation. Below the domes of the moiré pattern, the silicon atoms diffuse and grow as silicene nano flakes—a configuration of $\sqrt{3}\times\sqrt{3}$ silicene/3 × 3 Ru. The lattice of the silicene layer at the interface between graphene and Ru can be differentiated under certain bias voltages (Fig. 3(b)) [27]. Given the fact that the graphene lattice is single-crystalline and that the silicene lattice is locked to the Ru grain orientation, a twisting angle forms between the graphene and silicene lattice (Fig. S6 in the ESM).

After more silicon atoms are intercalated, the nano flakes connect with each other and form large scale silicene layer with a twisting angle to the top graphene layer with unchanged orientation (illustrated by the uninterrupted moiré pattern parameters of the adjacent part in Fig. 3(c)), i.e., TGS heterobilayers. The twisting angle is dependent on the grain orientation of the Ru grain. A typical TGS formed at the R37 region is displayed in Fig. 3(c). According to our density functional theory calculation, the TGS heterobilayer at the R37 region possesses a twisting angle of 4° between the graphene and the silicene lattices (Fig. 3(d)). The other possible heterobilayers are summarized in Table S1 and Fig. S7 in the ESM.

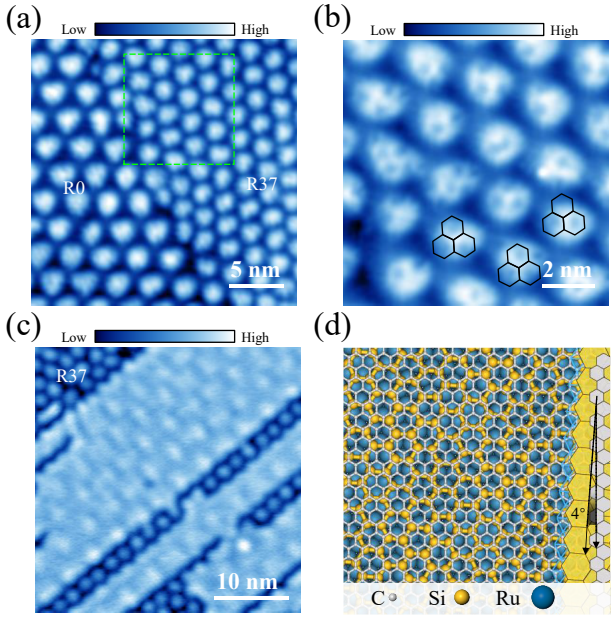

Figure 3 STM topography and atomic model of the TGS heterobilayers at the R37 region. (a) STM image of graphene intercalated with silicene nano flakes across the grain boundary between the R0 and R37 regions (V_s = −100 mV, I_t = 500 pA). (b) Zoom-in STM image of the R37 region in (a). Silicene nano flakes are indicated by black hexagons (V_s = −50 mV, I_t = 1000 pA). (c) STM image of the TGS heterobilayer at the R37 region after more Si atoms intercalate. (d) Atomic model of the TGS heterobilayer, showing a twisting angle of 4° between graphene and silicene.

We note that the different moiré patterns between graphene and Ru grains also influence the growth behavior of the silicene layer. Silicene growth at the interface starts from the nano flakes under the graphene moiré domes (atop sites) [31, 44]. At R0 region, the growth of silicene continues by occupying the graphene moiré valleys (face centered cubic (fcc) and hexagonal close packed (hcp) sites) and forms triangular islands [44]. At the TGS regions, however, silicene grows in a different manner. We take the R37 region as an example. After the moiré domes are intercalated by silicene nano flakes (Figs. 3(a) and 3(b)), further incoming silicon atoms tend to occupy the space between neighboring domes, forming silicene ribbons extending hundreds of nanometers in length (Fig. S5 in the ESM).

To understand the growth behavior of the silicene nanoribbon at the R37 region more clearly, DFT calculations were performed. When six Si atoms intercalate, they tend to locate at the fcc sites of the Ru (0001) surface, as shown in Fig. 4(a). Two incoming Si atoms tend to locate along the fcc-bridge direction (or $[11\bar{2}0]$ direction) (the formation energy is about 2 meV/Si lower than that along the hcp-bridge direction). If more Si atoms intercalate, the incoming Si atoms will further extend along the $[11\bar{2}0]$ direction between graphene and Ru (0001) surface, as shown in Figs. 4(a)–4(d). The direction is slightly off (by 11°) the high symmetry direction of the R37 moiré pattern. The confinement of the corrugated graphene thus sets constraints to the growth of the silicene at the interface, forming a wavy structure (Figs. 4(d) and 4(e)) which stabilizes the silicene nanoribbons.

In Fig. 4(f), we provide the formation energies per Si atom ($\Delta E(E_F) = (E_{total} - E_{moiré} - \mu_{Si}\times n)/n$, where E_{total} is the total energy of the graphene/silicene/Ru system, $E_{moiré}$ is the total energy of the moiré pattern, μ_{Si} is the chemical potential of the Si atom, and n is the number of the Si atoms) for different number of Si atoms in the R37 region. The orange dashed line indicates the formation energy of monolayer silicene in the R37 region ($2\sqrt{19}\times 2\sqrt{19}$ graphene/$\sqrt{21}\times\sqrt{21}$ silicene/$3\sqrt{7}\times 3\sqrt{7}$ Ru). From this figure, we can find that the formation energy decreases with the increasing of the intercalated Si atoms.

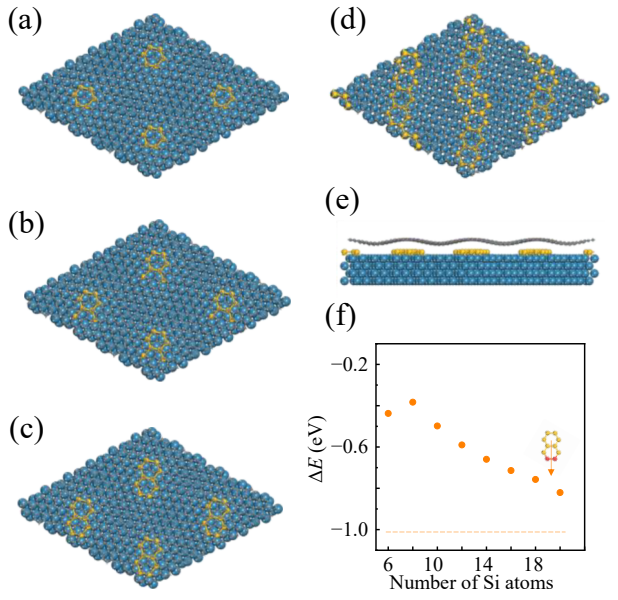

Figure 4 DFT calculation of the initial growth of the TGS bilayer at the R37 region. (a)–(e) Oriented growth of the silicene nanoribbons along [11$\bar{2}$0] direction between graphene and Ru (0001) surface. (e) is the side view of (d). (f) Si–Si bond energies of the silicene flakes with increasing number of Si atoms along [11$\bar{2}$0] direction. The orange dashed line shows the lower limit of Si–Si bond energy.

3 Conclusions

In conclusion, we have constructed TGS heterobilayers with different twisting angles by taking advantage of silicon intercalation between graphene and Ru substrate with multiple grains. The $3p_z$–$2p_z$ orbit hybridization may arouse the coupling of moiré super-lattices and topological band structures such as Dirac cone, flat band, and saddle points. Moreover, since intercalation phenomenon is commonly observed in epitaxial graphene systems, with recent progress in fabrication of large and controllable twinning metal substrates, our method could potentially be used to create graphene based twisted heterobilayers.

Acknowledgements

The work is supported by the Ministry of Science and Technology of China (Nos. 2019YFA0308500 and 2018YFA0305800), the National Natural Science Foundation of China (Nos. 61888102, 51991340, and 52072401), and the Chinese Academy of Sciences Project for Young Scientists in Basic Research (No. YSBR-003).

Electronic Supplementary Material: Supplementary material (large-scale STM images of R9–R19 region, STM and simulated images of R19 and R55 regions, STS in R0 and R37 regions, the property of single-crystalline across the grain boundary, and silicene nanoribbons at the R37 region) is available in the online version of this article at https://doi.org/10.1007/s12274-023-5408-5.

References

[1] Andrei, E. Y.; Efetov, D. K.; Jarillo-Herrero, P.; MacDonald, A. H.; Mak, K. F.; Senthil, T.; Tutuc, E.; Yazdani, A.; Young, A. F. The marvels of moiré materials. *Nat. Rev. Mater.* **2021**, *6*, 201–206.

[2] Andrei, E. Y.; MacDonald, A. H. Graphene bilayers with a twist. *Nat. Mater.* **2020**, *19*, 1265–1275.

[3] Cao, Y.; Fatemi, V.; Demir, A.; Fang, S.; Tomarken, S. L.; Luo, J. Y.; Sanchez-Yamagishi, J. D.; Watanabe, K.; Taniguchi, T.; Kaxiras, E. et al. Correlated insulator behaviour at half-filling in magic-angle graphene superlattices. *Nature* **2018**, *556*, 80–84.

[4] Cao, Y.; Fatemi, V.; Fang, S.; Watanabe, K.; Taniguchi, T.; Kaxiras, E.; Jarillo-Herrero, P. Unconventional superconductivity in magic-angle graphene superlattices. *Nature* **2018**, *556*, 43–50.

[5] Sharpe, A. L.; Fox, E. J.; Barnard, A. W.; Finney, J.; Watanabe, K.; Taniguchi, T.; Kastner, M. A.; Goldhaber-Gordon, D. Emergent ferromagnetism near three-quarters filling in twisted bilayer graphene. *Science* **2019**, *365*, 605–608.

[6] Park, J. M.; Cao, Y.; Watanabe, K.; Taniguchi, T.; Jarillo-Herrero, P. Flavour Hund's coupling, Chern gaps and charge diffusivity in moiré graphene. *Nature* **2021**, *592*, 43–48.

[7] Li, H. Y.; Li, S. W.; Regan, E. C.; Wang, D. Q.; Zhao, W. Y.; Kahn, S.; Yumigeta, K.; Blei, M.; Taniguchi, T.; Watanabe, K. et al. Imaging two-dimensional generalized Wigner crystals. *Nature* **2021**, *597*, 650–654.

[8] Kezilebieke, S.; Huda, M. N.; Vaňo, V.; Aapro, M.; Ganguli, S. C.; Silveira, O. J.; Głodzik, S.; Foster, A. S.; Ojanen, T.; Liljeroth, P. Topological superconductivity in a van der Waals heterostructure. *Nature* **2020**, *588*, 424–428.

[9] Xie, H. C.; Luo, X. P.; Ye, G. H.; Ye, Z. P.; Ge, H. W.; Sung, S. H.; Rennich, E.; Yan, S. H.; Fu, Y.; Tian, S. J. et al. Twist engineering of the two-dimensional magnetism in double bilayer chromium triiodide homostructures. *Nat. Phys.* **2022**, *18*, 30–36.

[10] Song, T. C.; Sun, Q. C.; Anderson, E.; Wang, C.; Qian, J. M.; Taniguchi, T.; Watanabe, K.; McGuire, M. A.; Stöhr, R.; Xiao, D. et al. Direct visualization of magnetic domains and moiré magnetism in twisted 2D magnets. *Science* **2021**, *374*, 1140–1144.

[11] Yankowitz, M.; Chen, S. W.; Polshyn, H.; Zhang, Y. X.; Watanabe, K.; Taniguchi, T.; Graf, D.; Young, A. F.; Dean, C. R. Tuning superconductivity in twisted bilayer graphene. *Science* **2019**, *363*, 1059–1064.

[12] Nimbalkar, A.; Kim, H. Opportunities and challenges in twisted bilayer graphene: A review. *Nano-Micro Lett.* **2020**, *12*, 126.

[13] Jiang, Y. H.; Lai, X. Y.; Watanabe, K.; Taniguchi, T.; Haule, K.; Mao, J. H.; Andrei, E. Y. Charge order and broken rotational symmetry in magic-angle twisted bilayer graphene. *Nature* **2019**, *573*, 91–95.

[14] Fournier, C.; Plaud, A.; Roux, S.; Pierret, A.; Rosticher, M.; Watanabe, K.; Taniguchi, T.; Buil, S.; Quélin, X.; Barjon, J. et al. Position-controlled quantum emitters with reproducible emission wavelength in hexagonal boron nitride. *Nat. Commun.* **2021**, *12*, 3779.

[15] Liao, M. Z.; Wu, Z. W.; Du, L. J.; Zhang, T. T.; Wei, Z.; Zhu, J. Q.; Yu, H.; Tang, J.; Gu, L.; Xing, Y. X. et al. Twist angle-dependent conductivities across MoS_2/graphene heterojunctions. *Nat. Commun.* **2018**, *9*, 4068.

[16] Liao, M. Z.; Wei, Z.; Du, L. J.; Wang, Q. Q.; Tang, J.; Yu, H.; Wu, F. F.; Zhao, J. J.; Xu, X. Z.; Han, B. et al. Precise control of the interlayer twist angle in large scale MoS_2 homostructures. *Nat. Commun.* **2020**, *11*, 2153.

[17] Zhang, X. Z.; Yang, H.; Hou, W. W.; Zheng, X. M.; Zhang, Y.; Zhang, R. Y.; Deng, C. Y.; Zhang, X. A.; Qin, S. Q. Twist-angle modulation of exciton absorption in MoS_2/graphene heterojunctions. *Appl. Phys. Lett.* **2019**, *115*, 181901.

[18] Wang, L.; Shih, E. M.; Ghiotto, A.; Xian, L. D.; Rhodes, D. A.; Tan, C.; Claassen, M.; Kennes, D. M.; Bai, Y. S.; Kim, B. et al. Correlated electronic phases in twisted bilayer transition metal dichalcogenides. *Nat. Mater.* **2020**, *19*, 861–866.

[19] Zhang, Z. M.; Wang, Y. M.; Watanabe, K.; Taniguchi, T.; Ueno, K.; Tutuc, E.; LeRoy, B. J. Flat bands in twisted bilayer transition metal dichalcogenides. *Nat. Phys.* **2020**, *16*, 1093–1096.

[20] Zhao, W. M.; Zhu, L.; Nie, Z. W.; Li, Q. Y.; Wang, Q. W.; Dou, L. G.; Hu, J. G.; Xian, L. D.; Meng, S.; Li, S. C. Moiré enhanced charge density wave state in twisted 1T-$TiTe_2$/1T-$TiSe_2$ heterostructures. *Nat. Mater.* **2022**, *21*, 284–289.

[21] Zhu, Y. Y.; Liao, M. H.; Zhang, Q. H.; Xie, H. Y.; Meng, F. Q.; Liu, Y. W.; Bai, Z. H.; Ji, S. H.; Zhang, J.; Jiang, K. L. et al. Presence of *s*-wave pairing in Josephson junctions made of twisted ultrathin $Bi_2Sr_2CaCu_2O_{8+x}$ flakes. *Phys. Rev. X* **2021**, *11*, 031011.

[22] Wang, Y. Y.; Ni, Z. Y.; Liu, Q. H.; Quhe, R.; Zheng, J. X.; Ye, M.; Yu, D. P.; Shi, J. J.; Yang, J. B.; Li, J. et al. All-metallic vertical transistors based on stacked dirac materials. *Adv. Funct. Mater.* **2015**, *25*, 68–77.

[23] Peymanirad, F.; Neek-Amal, M.; Beheshtian, J.; Peeters, F. M. Graphene-silicene bilayer: A nanocapacitor with permanent dipole and piezoelectricity effect. *Phys. Rev. B* **2015**, *92*, 155113.

[24] Molle, A.; Grazianetti, C.; Tao, L.; Taneja, D.; Alam, M. H.; Akinwande, D. Silicene, silicene derivatives, and their device applications. *Chem. Soc. Rev.* **2018**, *47*, 6370–6387.

[25] Geim, A. K.; Grigorieva, I. V. Van der Waals heterostructures. *Nature* **2013**, *499*, 419–425.

[26] Li, G.; Zhang, Y. Y.; Guo, H.; Huang, L.; Lu, H. L.; Lin, X.; Wang, Y. L.; Du, S. X.; Gao, H. J. Epitaxial growth and physical properties of 2D materials beyond graphene: From monatomic materials to binary compounds. *Chem. Soc. Rev.* **2018**, *47*, 6073–6100.

[27] Li, G.; Zhang, L. Z.; Xu, W. Y.; Pan, J. B.; Song, S. R.; Zhang, Y.; Zhou, H. T.; Wang, Y. L.; Bao, L. H.; Zhang, Y. Y. et al. Stable silicene in graphene/silicene van der Waals heterostructures. *Adv. Mater.* **2018**, *30*, 1804650.

[28] Guo, H.; Zhang, R. Z.; Li, H.; Wang, X. Y.; Lu, H. L.; Qian, K.; Li, G.; Huang, L.; Lin, X.; Zhang, Y. Y. et al. Sizable band gap in epitaxial bilayer graphene induced by silicene intercalation. *Nano Lett.* **2020**, *20*, 2674–2680.

[29] Ben Jabra, Z.; Abel, M.; Fabbri, F.; Aqua, J. N.; Koudia, M.; Michon, A.; Castrucci, P.; Ronda, A.; Vach, H.; De Crescenzi, M. et al. Van der Waals heteroepitaxy of air-stable quasi-free-standing silicene layers on CVD epitaxial graphene/6H-SiC. *ACS Nano* **2022**, *16*, 5920–5931.

[30] Pan, Y.; Shi, D. X.; Gao, H. J. Formation of graphene on Ru (0001) surface. *Chin. Phys.* **2007**, *16*, 3151–3153.

[31] Pan, Y.; Zhang, H. G.; Shi, D. X.; Sun, J. T.; Du, S. X.; Liu, F.; Gao, H. J. Highly ordered, millimeter-scale, continuous, single-crystalline graphene monolayer formed on Ru (0001). *Adv. Mater.* **2009**, *21*, 2777–2780.

[32] Sutter, E.; Albrecht, P.; Sutter, P. Graphene growth on polycrystalline Ru thin films. *Appl. Phys. Lett.* **2009**, *95*, 133109.

[33] Zhang, L. N.; Dong, J. C.; Guan, Z. Y.; Zhang, X. Y.; Ding, F. The alignment-dependent properties and applications of graphene moiré superstructures on the Ru (0001) surface. *Nanoscale* **2020**, *12*, 12831–12839.

[34] Wu, Z. B.; Gao, Z. Y.; Chen, X. Y.; Xing, Y. Q.; Yang, H.; Li, G.; Ma, R. S.; Wang, A. W.; Yan, J. H.; Shen, C. M. et al. A low-temperature scanning probe microscopy system with molecular beam epitaxy and optical access. *Rev. Sci. Instrum.* **2018**, *89*, 113705.

[35] Becker, R. S.; Golovchenko, J. A.; Swartzentruber, B. S. Electron interferometry at crystal surfaces. *Phys. Rev. Lett.* **1985**, *55*, 987–990.

[36] Kresse, G.; Furthmüller, J. Efficient iterative schemes for *ab initio* total-energy calculations using a plane-wave basis set. *Phys. Rev. B* **1996**, *54*, 11169–11186.

[37] Kresse, G.; Furthmüller, J. Efficiency of *ab-initio* total energy calculations for metals and semiconductors using a plane-wave basis set. *Comput. Mater. Sci.* **1996**, *6*, 15–50.

[38] Blöchl, P. E. Projector augmented-wave method. *Phys. Rev. B* **1994**, *50*, 17953–17979.

[39] Perdew, J. P.; Burke, K.; Ernzerhof, M. Generalized gradient approximation made simple. *Phys. Rev. Lett.* **1996**, *77*, 3865–3868.

[40] Sutter, P. W.; Flege, J. I.; Sutter, E. A. Epitaxial graphene on ruthenium. *Nat. Mater.* **2008**, *7*, 406–411.

[41] Ophus, C.; Shekhawat, A.; Rasool, H.; Zettl, A. Large-scale experimental and theoretical study of graphene grain boundary structures. *Phys. Rev. B* **2015**, *92*, 205402.

[42] Zhang, H. G.; Hu, H.; Pan, Y.; Mao, J. H.; Gao, M.; Guo, H. M.; Du, S. X.; Greber, T.; Gao, H. J. Graphene based quantum dots. *J. Phys. Condens. Matter* **2010**, *22*, 302001.

[43] Meng, L.; Wu, R. T.; Zhang, L. Z.; Li, L. F.; Du, S. X.; Wang, Y. L.; Gao, H. J. Multi-oriented moiré superstructures of graphene on Ir (111): Experimental observations and theoretical models. *J. Phys. Condens. Matter* **2012**, *24*, 314214.

[44] Li, G.; Zhou, H. T.; Pan, L. D.; Zhang, Y.; Huang, L.; Xu, W. Y.; Du, S. X.; Ouyang, M.; Ferrari, A. C.; Gao, H. J. Role of cooperative interactions in the intercalation of heteroatoms between graphene and a metal substrate. *J. Am. Chem. Soc.* **2015**, *137*, 7099–7103.

[45] Gao, Z. Y.; Xu, W. P.; Gao, Y. X.; Guzman, R.; Guo, H.; Wang, X. Y.; Zheng, Q.; Zhu, Z. L.; Zhang, Y. Y.; Lin, X. et al. Experimental realization of atomic monolayer Si_9C_{15}. *Adv. Mater.* **2022**, *34*, 2204779.